

Article

Estimation and Mapping of Actual and Potential Grassland Root Carbon Storage: A Case Study in the Altay Region, China

Fangzhen Li ^{1,2,3} , Huaping Zhong ², Kehui Ouyang ⁴, Xiaomin Zhao ^{1,3,*} and Yuzhe Li ^{2,*}¹ School of Land Resource and Environment, Jiangxi Agricultural University, Nanchang 330045, China² Key Laboratory of Land Surface Pattern and Simulation, Institute of Geographic Sciences and Natural Resources Research, Chinese Academy of Sciences, Beijing 100101, China³ Key Laboratory of Poyang Lake Watershed Agricultural Resources and Ecology of Jiangxi Province, Nanchang 330045, China⁴ School of Animal Science and Technology, Jiangxi Agricultural University, Nanchang 330045, China

* Correspondence: zhaoxm889@126.com (X.Z.); liyuzhe@igsnr.ac.cn (Y.L.)

Abstract: The actual root carbon storage (ARCS) and potential root carbon storage (PRCS) of grasslands play an important role in the global carbon balance and carbon neutralization. However, estimation of these indicators is difficult. In addition, their spatial patterns and crucial driving factors also require clarification. In this study, an approach for accurate estimation of ARCS and PRCS was developed incorporating a support vector machine model and high-accuracy surface modeling. Based on field data collected from Altay Prefecture in 2015, the estimation accuracy (R^2) of root biomass in the 0–10, 10–20, and 20–30 cm soil layers of grassland were 0.73, 0.63, and 0.60, respectively. In addition, the spatial patterns of actual root carbon density (ARCD) and potential root carbon density (PRCD) were analyzed. The ARCD increased with the increase in elevation. High PRCD was located on hillsides with a gentle slope. The dominant interaction factors for the ARCD spatial pattern were temperature and precipitation, whereas the main interaction factors for the PRCD pattern were temperature and slope. The grassland ARCS and PRCS in Altay Prefecture were estimated to be 48.52 and 22.69 Tg C, respectively. We suggest there is considerable capacity to increase grassland ARCS in the study area.

Keywords: root carbon storage; potential storage; grassland; HASM; Altay Prefecture

Citation: Li, F.; Zhong, H.; Ouyang, K.; Zhao, X.; Li, Y. Estimation and Mapping of Actual and Potential Grassland Root Carbon Storage: A Case Study in the Altay Region, China. *Agronomy* **2022**, *12*, 2632. <https://doi.org/10.3390/agronomy12112632>

Academic Editors: Xiaoping Xin, Xiao Sun, Xianglin Li and Dawei Xu

Received: 24 August 2022

Accepted: 24 October 2022

Published: 26 October 2022

Publisher's Note: MDPI stays neutral with regard to jurisdictional claims in published maps and institutional affiliations.



Copyright: © 2022 by the authors. Licensee MDPI, Basel, Switzerland. This article is an open access article distributed under the terms and conditions of the Creative Commons Attribution (CC BY) license (<https://creativecommons.org/licenses/by/4.0/>).

1. Introduction

Plant carbon storage is a crucial component of the terrestrial ecosystem carbon cycle. The carbon sequestration by terrestrial plants is limited compared with soil carbon storage [1]. However, soils cannot fix CO₂ actively; this function is entirely undertaken by plants. Plants fix CO₂ from the atmosphere through photosynthesis and store a portion of the organic carbon in the soil through their roots [2,3]. Therefore, plants are important contributors to soil organic carbon stocks in terrestrial ecosystems [4,5].

In grassland ecosystems, plant carbon storage is mainly concentrated in the roots rather than in photosynthetic organs. The root biomass accounts for 70–85% of the total biomass [6]. Thus, root carbon storage largely determines the overall capacity for plant carbon storage in grasslands [7,8]. This is quantified as the actual root carbon storage (ARCS). To address the global dilemma of carbon emission and storage, it is necessary to calculate the potential carbon holding capacity of roots. However, no standardized definition of potential carbon storage is accepted universally. Current research primarily refers to the difference between the peak carbon storage, which could be achieved through climate change and management measures, and the actual carbon storage [9]. Therefore, potential root carbon storage (PRCS) is defined as the holding capacity of grassland root carbon storage that can be improved in the future.

Carbon storage in the photosynthetic organs of grasslands can be reliably estimated from remote sensing data [10–12], but it remains difficult to estimate storage in below-ground biomass. Estimation of the ARCS of grassland ecosystems is pivotal to understand the global carbon cycle. Traditionally, three major approaches have been used to estimate ARCS over large spatial domains. One strategy is to simulate the carbon cycle process in a grassland ecosystem by using a macroscopic biogeochemical model to derive ARCS [13,14]. In China, the national grassland ARCS has been estimated as 1.85 and 2.78 Pg C using the Denitrification–Decomposition Model and the Terrestrial Ecosystem Model, respectively. Divergent parameters and differences in spatial resolution of the two models account for the discrepancy in results, even if the parameters with the highest correlation coefficients are used in the models [15,16]. A second approach is to estimate aboveground biomass from remotely sensed images and then derive ARCS based on empirical root: shoot ratios [17]. However, multiple uncertainties reduce the credibility of the outputs. Third, the actual root carbon density (ARCD) is estimated using root biomass and carbon content from sample data. Subsequently, the ARCS is derived by multiplying ARCD and the area. However, the field investigation required in the initial step of this approach is time and labor intensive [18].

Assessment of potential carbon storage is an additional aspect of carbon cycle research [19–21]. Such assessment plays an important role in optimizing current ecological management measures and formulating future environmental management strategies [22,23]. Several approaches have been used to estimate the peak carbon storage. Temporal- and spatial-based methods have been used in ecosystems. Temporal methods rely on time-series changes in carbon storage for determination of the peak value [24]. This approach is a popular means of predicting potential carbon storage. The spatial approach is premised on the theory of natural succession of ecosystems [25]. The accessible carbon storage is considered to be maximal when all types of plants have attained their highest succession stage. Both methods have been used for estimation of potential carbon storage in soils but rarely to estimate that in roots.

In recent years, maintenance of the ARCS capacity and functions in grassland has been challenged by climate change and human activities. If grasslands shrink in area, even slightly, it will immediately affect the capacity of grassland soils to store organic carbon, putting enormous pressure on the global carbon balance and carbon neutrality [26]. Currently, research on ARCS and PRCS in central Asian grasslands is limited [27].

In this study, a typical grassland region of central Asia was selected to study the spatial patterns and key spatial drivers of ARCS and PRCS in grassland based on a field survey conducted in 2015. The study area is located near the Altai Mountains and contains seven types of grassland, ranging from temperate desert in arid and semi-arid areas to alpine meadow. The dominance of grassland in the region provides an ideal simulation test area for grassland root carbon research. In practice, conducting large-scale field surveys of grassland roots in complex terrain is time consuming and impractical. Therefore, the present research aimed to improve the feasibility of studying root carbon storage. The objectives of this study were three-fold: (1) to develop an approach to estimate and map grassland root biomass in complex terrain with improved accuracy in relation to ecological and topographic factors; (2) to examine the spatial characteristics of ARCD and PRCD of grassland in areas where multiple grassland types coexist; and (3) to analyze the crucial spatial drivers of ARCS and PRCS of the grasslands.

2. Materials and Methods

2.1. Study Area

Altay Prefecture (45°00′00″–49°10′45″ N, 85°31′36″–91°04′23″ E) is located in the southern foothills of the Altai Mountains in northwest China (Figure 1). It is a typical area in central Asia with a total land area of 1.18×10^5 km². Two main landforms, namely mountains and plains, coexist in the area. The climate is cold-temperate continental, with mean annual temperature of 4.5 °C and mean monthly temperature ranging from –16 °C

in January to 21 °C in July. It is an arid to semi-arid area with mean annual precipitation of 200 mm (400–600 mm in the mountains) and evaporation of 1682.6 mm yr⁻¹. The terrain exhibits a low-to-high gradient from south to north with obvious spatial heterogeneity. The grasslands comprise lowland meadow, temperate desert, temperate desert steppe, temperate steppe, temperate meadow, mountain meadow, and alpine meadow. The dominant species are *Achnatherum splendens*, *Seriphidium terrae-albae*, *Stipa glareosa*, *Agropyron cristatum*, *Stipa capillata*, *Poa versicolor* subsp. *relaxa*, and *Carex duriuscula* subsp. *rigescens*. Temperate desert accounts for 67% of the total grassland area.

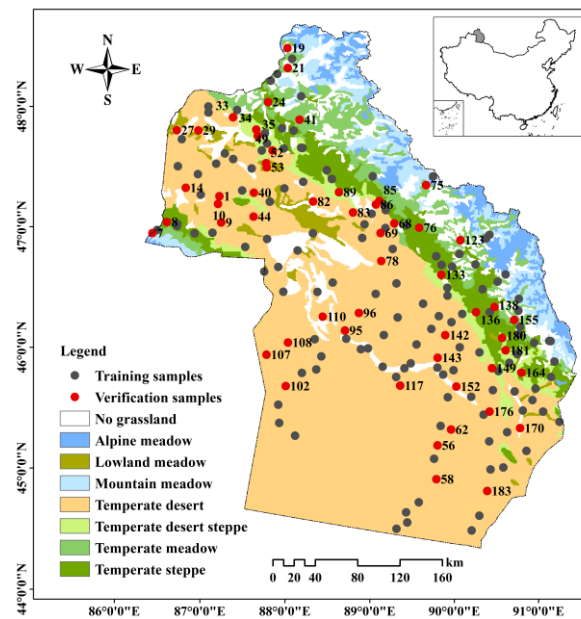


Figure 1. Sampling locations and grassland types in Altay Prefecture, China.

2.2. Data

2.2.1. Field Survey Data

With consideration of the different grassland types and human disturbance, 187 sites (10 m × 10 m) were randomly established across Altay Prefecture during the growing season (June to August) of 2015. When sampling, three replicate plots were sampled from a diagonal line of each site with similar topographical conditions, soil attributes, and grassland types. The distance between plots at a site was more than 2 m. Meanwhile, three samples were collected from the 0–10 cm, 10–20 cm, and 20–30 cm soil layers at each site. In total, 187 plant samples (green part) and 561 soil samples were collected. The recorded field data comprised the longitude, latitude, and elevation of the sampling site confirmed by GPS and the type, height, coverage, root biomass, and soil bulk density of the grassland. Height was represented by the relative altitude and was measured with a tape measure. Field coverage was determined using the square grid method, which was calculated as the ratio of grass grids to the total number of grids. For measurement of the root biomass at each site, soil samples were collected at depths of 0–10 cm, 10–20 cm, and 20–30 cm and placed separately in plastic bags. Each soil sample was transferred to a 60-mesh nylon bag (0.3 mm) and washed with running water. The roots were collected with a 60-mesh sieve (0.3 mm), oven-dried at 65 °C for 48 h, and the dry weight was recorded to measure root biomass. The soil bulk density of the 0–10, 10–20, and 20–30 cm soil layers was determined using the ring knife method to collect soil core samples, which were dried at 105 °C for 48 h.

2.2.2. Terrain and Climate Data

The slope, aspect, and curvature of the terrain were determined from advanced spaceborne thermal emission and reflect radiometer global digital elevation (ASTER GDEM) images obtained from the Land Process Distributed Active Archiving Center (LP DAAC)

(<https://lpdaac.usgs.gov/>, accessed on 20 August 2022) with spatial resolution of 30 m. Meteorological data were obtained from weather stations of the China Meteorological Information Center (<http://data.cma.cn/en>, accessed on 20 August 2022), consisting of annual mean temperature, ≥ 10 °C accumulated temperature, annual mean precipitation, and moisture index, with spatial resolution of 1 km. Ivanov's moisture index was calculated using the following formula:

$$K = \frac{R}{E_0} = \frac{R}{\sum_{i=1}^{12} 0.0018(25 + t_i)^2(100 - f_i)} \quad (1)$$

where K is annual humidity, R is annual precipitation, E_0 is annual evaporation, t_i is monthly average temperature, and f_i is monthly average evaporation.

2.2.3. Remote Sensing Data

Three remote sensing indices were applied in this research: normalized difference vegetation index (NDVI), enhanced vegetation index (EVI), and soil-adjusted vegetation index (SAVI). The NDVI comprised the composite data sensed by the medium-resolution imaging spectrometer (MOD13Q1) obtained from NASA (<https://ladsweb.modaps.eosdis.nasa.gov/>, accessed on 20 August 2022) with spatial resolution of 1 km. The EVI and SAVI were extracted from Landsat8OLI satellite images with spatial resolution of 30 m from the Geospatial Data Cloud (<http://www.gscloud.cn/>, accessed on 20 August 2022) using ENVI image analysis software. All remote sensing index data were collected in the peak season of plant growth in 2015 (day 255) and obtained using the following respective formulas:

$$NDVI = \frac{NIR - R}{NIR + R} \quad (2)$$

$$EVI = 2.5 \frac{NIR - R}{NIR + 6R - 7.5B + 1} \quad (3)$$

$$SAVI = \frac{NIR - R}{NIR + R + L} (1 + L), (L = 0.5) \quad (4)$$

where NIR, R, and B represent the reflectance in the near-infrared band, red band, and blue band, respectively, and L is the soil adjustment factor.

2.2.4. Thematic Map Data

Other data used in this research were soil textures and grassland types in Altay Prefecture, which were obtained from the resource and environmental data cloud platform of the Chinese Academy of Sciences (<http://www.resdc.cn/>, accessed on 20 August 2022).

2.3. Spatial Estimation of Grassland Root Biomass

2.3.1. Correlation Analysis and Indicator Selection

Outliers were identified with box plots and were eliminated during data preprocessing to ensure the quality of the data. Box plots can truly and intuitively present the original appearance of the data, and objectively identify outliers based on quartiles and interquartile ranges [28,29]. In this study, two outliers were identified and eliminated, which may be due to sampling error. Subsequently, a Pearson correlation analysis was performed between the 185 field samples and 19 ecological factors. The threshold for the correlation test (r) was $-0.75 < r < 0.75$ (Table 1). With increase in soil depth, the correlation between root biomass and most ecological factors weakened gradually. In addition, nine ecological factors with applied relevance were selected ($|r| > 0.60$) as independent variables for the model building of the root biomass prediction: elevation, slope, temperature, accumulated temperature, precipitation, moisture, soil bulk density, coverage, and NDVI.

Table 1. Correlation coefficients (r) between grassland root biomass and ecological factors.

Items	Indices	Soil Layers		
		0–10 cm	10–20 cm	20–30 cm
Position	Latitude	0.49 **	0.49 **	0.49 **
	Longitude	−0.18 *	−0.18 *	−0.21 **
Terrain	Altitude	0.66 **	0.65 **	0.62 **
	Slope	0.63 **	0.61 **	0.61 **
	Aspect	−0.04	−0.09	−0.09
	Curvature	−0.11	−0.08	−0.05
Climate	Precipitation	0.71 **	0.70 **	0.69 **
	Temperature ≥10 °C	−0.70 **	−0.69 **	−0.65 **
	Accumulated temperature	−0.75 **	−0.73 **	−0.70 **
	Moisture	0.75 **	0.73 **	0.72 **
Soil	Clay	0.39 **	0.40 **	0.40 **
	Sand	−0.24 **	−0.26 **	−0.24 **
	Silt	0.08	0.10	0.08
	Density	−0.74 **	−0.73 **	−0.72 **
Plant	Coverage	0.72 **	0.71 **	0.68 **
	Height	0.04	0.02	0.02
	NDVI	0.67 **	0.65 **	0.60 **
	EVI	0.58 **	0.58 **	0.52 **
	SAVI	0.50 **	0.47 **	0.41 **

Note: * $p < 0.05$, ** $p < 0.01$.

2.3.2. Data Segmentation and Statistics

Reasonable data segmentation involves generating training datasets and validation datasets to ensure that they present similar statistical features [30,31]. This process is a foundation for reliable model building. In this research, the training dataset ($n = 130$, 70%) and the validation dataset ($n = 55$, 30%) were obtained by holistic ordinary least squares regression. Their mathematical parameters were further counted (Table 2). The biomass of grassland roots ranged from 28.85 to 2485.20 g m^{-2} in the 0–30 cm soil layer. The biomass decreased with soil depth. In the 0–10 cm soil layer, the root biomass was 169.87–2485.20 g m^{-2} with a mean value of 809.57 g m^{-2} and SD of 511.81 g m^{-2} . In the 10–20 cm soil layer, root biomass was 104.76–862.95 g m^{-2} with a mean value of 328.31 g m^{-2} and SD of 167.33 g m^{-2} . The lowest root biomass was in the 20–30 cm soil layer, with a mean value of 155.61 g m^{-2} and SD of 94.40 g m^{-2} . The training data showed a unimodal and skewed distribution. The skewness coefficients were 0.96, 0.84, and 0.95 for the 0–10 cm, 10–20 cm, and 20–30 cm soil layers. The verification data showed a unimodal, skewed distribution. Their mathematical parameters were similar in the 0–30 cm soil layer. In addition, the skewness coefficients were greater than zero. They showed some slightly higher values mixing in datasets of root biomass.

Table 2. Descriptive statistics for grassland root biomass in the training data and verification data (g m^{-2}).

	Training Data (n = 130)			Verification Data (n = 55)		
	0–10 cm	10–20 cm	20–30 cm	0–10 cm	10–20 cm	20–30 cm
Min	180.68	107.42	29.46	169.87	104.76	28.85
Max	2485.20	862.95	471.45	2401.21	808.69	484.32
Mean	809.57	329.10	153.45	809.65	326.44	160.72
SD	511.81	167.33	94.40	510.83	172.40	110.36
Median	640.69	270.35	127.52	648.58	266.06	132.93
Skewness	0.96	0.84	0.95	1.15	0.91	0.93

2.3.3. Estimation Models and Spatial Interpolation Methods

Machine learning is a scientific discipline that involves the construction and study of algorithms that can learn from data [32]. As the core of artificial intelligence, machine learning has been widely used to solve complex problems in engineering applications and science [33–36]. In this study, three machine-learning models were used to estimate root biomass, comprising support vector machine (SVM), principal component regression (PCR), and random forest (RF). Based on statistical principles, SVM seeks to minimize the risk of structural learning to improve the generalization ability of the learning machine and achieve the purpose of obtaining statistical laws when the sample size is small. It can solve data problems, such as small sample sizes, nonlinearity, and high dimensionality [37]. PCR extracts principal components that rely on the variance, and then performs regression based on the principal components. The approach can handle massive datasets and data dimensionality reduction [38,39]. An RF composed of multiple decision trees is a representative model of integrated learning. The final output is determined by each decision tree in the forest. The method can overcome the problems of overfitting and low precision of decision trees and is suitable for the prediction of high-dimensional data [40,41]. In the present study, SVM and PCR were implemented with The Unscrambler X 10.4, and RF was implemented with R 4.1.1.

Spatial interpolation can convert measured data from discrete points into continuous data surfaces, which is the main method used to achieve the spatialization of point data [42,43]. Previous studies have shown that field-measured data cannot adequately reflect spatial changes in the target, even if the data are of high quality. In the present research, the spatial interpolation methods used were high accuracy surface modeling (HASM), radial basis function (RBF), and spline with tension (SPL). Based on the existing spatial interpolation results, HASM superimposes the optimized residual surface to obtain the surface of the target [44]. RBF is based on characterizing the localized features of the data by introducing a kernel function [45]. SPL relies on polynomial fitting to generate smooth interpolated surfaces. The loss of accuracy is inevitable, although these spatial interpolations enable surface creation from point data. In this study, HASM was implemented with Matlab 2014b, and RBF and SPL were implemented with ArcGIS 10.7.

The regression prediction of the sample data was realized with multivariate environmental factors combined with a machine-learning model. Based on the prediction results, the spatial interpolation method was then used for two-dimensional surface creation from one-dimensional data. An optimal combination of the estimation model and spatial interpolation was determined for estimation and mapping of the root biomass of the grasslands.

2.3.4. Accuracy

Simultaneously, the prediction results obtained from the optimal combination were compared with the measured values. The accuracy of the target was determined by univariate linear regression. The estimated accuracy, as reflected by the coefficient of determination (R^2), root mean squared error (RMSE), and mean absolute error (MAE), relied on the verification data (30% of the total data). The values of R^2 , RMSE, and MAE were calculated with the formulas:

$$R^2 = \frac{SSR}{SST} = \frac{\sum_{i=1}^N (t_i - \bar{t})^2}{\sum_{i=1}^N (T_i - \bar{t})^2} \quad (5)$$

$$RMSE = \sqrt{\frac{\sum (t_i - T_i)^2}{N}} \quad (6)$$

$$MAE = \frac{1}{N} \sum_{i=1}^N |T_i - t_i| \quad (7)$$

where SSR and SST are the explained sum of squares regression and the total sum of squares, respectively; t_i , \bar{t} , and T_i are the measured value, mean measured value, and estimated value, respectively; and N is the size of the verification dataset.

2.4. Estimation of ARCS and PRCS of Grasslands

2.4.1. Calculation of ARCS

Determination of the carbon content coefficient is crucial to the conversion from root biomass to ARCD. Universally, the carbon coefficient of plants used internationally is 0.45 [6,46]. The coefficient is widely applied in the carbon density conversion for different plants and plant organs. The carbon content of grass roots in deep soil layers is higher than that in the surface soil layer. Therefore, it is infeasible to use a single carbon content coefficient to convert the carbon density of different soil layers, which will amplify the error of the calculated carbon storage. In the present research, different carbon content coefficients were used in the conversion of the ARCD in different soil layers according to their outcome [47]. In addition, the ARCS was determined by multiplying the ARCD and area. The respective formulas used were:

$$ARCD = \frac{1}{n} \sum_{i=1}^n (RB_{ij} \times \omega_j), (j = 1, 2, 3) \quad (8)$$

$$ARCS = \sum (ARCD \times k) \quad (9)$$

where ARCD and ARCS are actual root carbon density and actual root carbon storage of the grassland, respectively; RB is root biomass; ω is the carbon content coefficient, which is 0.38, 0.40, and 0.42 in the 0–10 cm, 10–20 cm, and 20–30 cm soil layers, respectively; i is the sample number; j is the depth of the soil layer, where j_1 to j_3 are the 0–10 cm, 10–20 cm, and 20–30 cm soil layers; n is the sample size; and k is the area.

2.4.2. Calculation of PRCS

A spatial segmentation approach was employed to calculate the PRCS of the grassland. First, the largest ARCD of the investigated data in each grassland type was regarded as the peak value. The potential root carbon density (PRCD) was then defined as the mean distance between the peak value and other values. In this study, the PRCS was determined by multiplying the PRCD and area. The respective formulas used were:

$$PRCD = \frac{1}{n} \sum_{i=1}^n (ARCD_{\max} - ARCD) \quad (10)$$

$$PRCS = \sum (PRCD \times k) \quad (11)$$

where PRCD and PRCS are potential root carbon density and potential root carbon storage of the grassland, respectively; $ARCD_{\max}$ is the peak value of ARCD; i is the sample number; n is the sample size; and k is the area.

2.5. Drivers of Spatial Pattern

The information from the sample sites was re-extracted to explain the formation of patterns in the grasslands of Altay Prefecture. In the present research, the process of indicator selection and correlation testing were run again to obtain the dominant drivers. Equation fitting was employed to determine their trends. Simultaneously, the impact of the interaction between ecological factors on the target cannot be ignored. Thus, the functions for factor detection and interaction detection implemented in the Geodetector software (2015) were employed to identify the dominant interaction factors in the formation of the spatial pattern of root carbon storage. Geodetector is a statistical method for detection of spatial heterogeneity and its driving factors [48]. The contribution of partial variance to the integral variance is identified as the interpretation ability of variables to the target. The

q-value ranges from 0 to 1 and aids in understanding spatial confounding, sample bias, and overfitting. The higher the q-value, the stronger the interpretation ability.

3. Results

3.1. An Optimal Approach for Spatial Estimation of Root Biomass

An optimal approach for estimation and mapping of grassland root biomass was developed by the combination of a machine-learning model and spatial interpolation method, designated SVM + HASM. The estimation for the 0–10 cm soil layer is presented as an example (Table 3). Compared with the PCR and RF models, the SVM model achieved higher accuracy and a smaller error ($R^2 = 0.74$, $RMSE = 259.66 \text{ g m}^{-2}$, and $MAE = 213.58 \text{ g m}^{-2}$). The SVM model offered the strongest foundation for the following spatial interpolation. Generally, digital mapping through spatial interpolation will further decrease the accuracy. Accordingly, a small loss in accuracy indicates a superior interpolation function. In the present research, the loss in accuracy of R^2 with HASM was 0.01–0.02, whereas R^2 declined about 5–10 times that of HASM with the RBF and SPL methods by 0.04–0.08 and 0.06–0.10, respectively. In addition, HASM resulted in the lowest error. These results indicated that HASM provided an excellent function for mapping. In this study, SVM and HASM performed best for estimation and mapping, respectively. The combination of the two methods generated the optimal results ($R^2 = 0.73$, $RMSE = 273.84 \text{ g m}^{-2}$, and $MAE = 213.61 \text{ g m}^{-2}$). Therefore, the spatial pattern of root biomass in the 10–20 cm and 20–30 cm soil layers was estimated with $R^2 = 0.63$ and $R^2 = 0.60$, respectively, with this combination.

Table 3. Accuracy of different combinations of estimation models and spatial interpolation methods for mapping of grassland root biomass in the 0–10 cm soil layer in Altay Prefecture, China.

Machine-Learning Models	Spatial Interpolation Method	0–10 cm		
		R^2	RMSE	MAE
SVM	-	0.74	259.66	213.58
	HASM	0.73	273.84	213.61
	RBF	0.66	289.70	244.46
	SPL	0.64	317.84	260.13
PCR	-	0.72	275.18	231.37
	HASM	0.70	282.66	222.63
	RBF	0.66	296.96	250.13
	SPL	0.65	305.84	259.19
RF	-	0.70	282.75	234.21
	HASM	0.69	284.39	224.92
	RBF	0.66	300.88	253.80
	SPL	0.64	309.32	258.88

3.2. Spatial and Statistical Pattern of ARCD and ARCS in Grassland

Based on the stratified carbon content of the roots, the two-dimensional surface of ARCD in the 0–30 cm soil layer was generated, and the spatial pattern was studied further. The spatial pattern of ARCD in the different soil layers was similar in the study area (Figure 2a–c). Horizontally, the ARCD was concentrated in the north and sparse in the south. With regard to the vertical spatial pattern, the ARCD was higher at mountainous sites than that of plains. Specifically, the high-value areas of ARCD were principally located on the southern slopes of the Altai Mountains in northern Altay Prefecture. In addition, high ARCD values were distributed on the northern slopes of the Sawuer Mountains in western Altay Prefecture. The low-value areas were situated in the Gurbantunggut Desert and central Altay Prefecture. In the 0–30 cm soil layer, the mean ARCD of grassland in Altay Prefecture was $499.24 \text{ g C m}^{-2}$ and the ARCS was 48.52 Tg C . In the topsoil (0–10 cm), the ARCD was $305.07 \text{ g C m}^{-2}$ and the ARCS was 29.42 Tg C , comprising approximately

61% of the total ARCS. In the 10–20 cm and 20–30 cm soil layers, the ARCS was 12.85 and 6.86 Tg C, respectively, comprising 26% and 13% of the total ARCS.

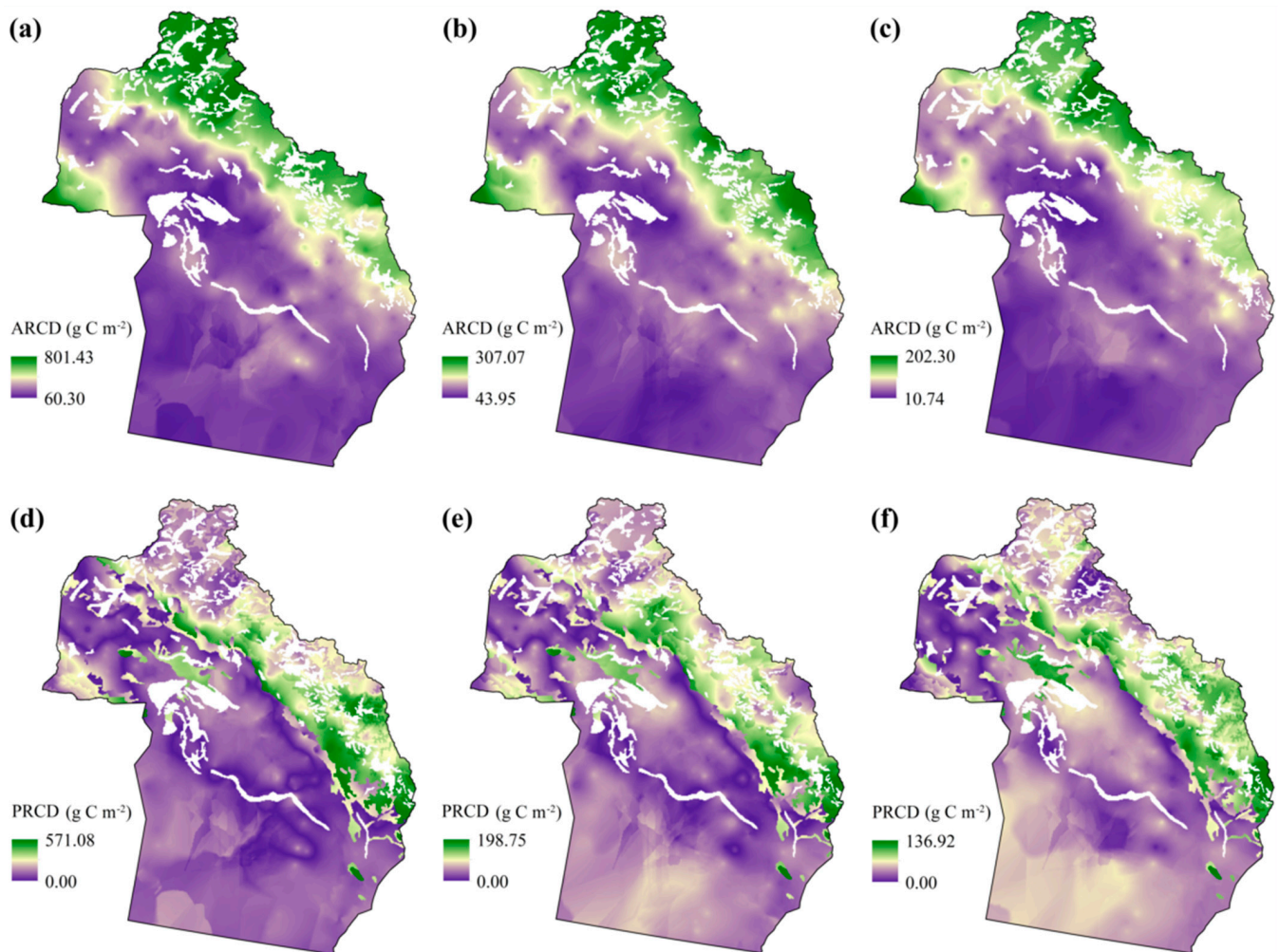


Figure 2. Spatial patterns of grassland actual root carbon density (ARCD) and potential root carbon density (PRCD) in Altay Prefecture. (a–c) Spatial pattern of ARCD in the 0–10 cm, 10–20 cm, and 20–30 cm soil layers, respectively; (d–f) spatial pattern of PRCD in the 0–10 cm, 10–20 cm, and 20–30 cm soil layers, respectively.

The ARCD and ARCS of the different types of grasslands were estimated (Figure 3a,b). In the 0–30 cm soil layer, temperate desert retained the largest ARCS of 19.15 Tg C, comprising 39.49% of the total ARCS, although it contained the lowest ARCD in each soil layer. Lowland meadow retained the smallest ARCS of 1.25 Tg C, which comprised 2.58% of the total. Alpine meadow had the highest ARCD with 1264.73 g C m⁻², whereas its ARCS was 5.98 Tg C (12.32% of the total).

3.3. Spatial and Statistical Patterns of PRCD and PRCS in Grassland

The spatial pattern of PRCD in the different soil layers was similar in Altay Prefecture (Figure 2d–f). The high-value areas of PRCD were located in the border topography at mid to high elevations. They were principally situated on the middle of the southern slopes of the Altai Mountains at elevations ranging from 1000 to 2200 m. In addition, areas of high PRCD were sporadically distributed near water at low elevations. Overall, the area of high PRCD was significantly less than that of low PRCD in Altay Prefecture. In the 0–30 cm soil layer, the mean PRCD of grassland in Altay was 247.12 g C m⁻² and the mean PRCS was 22.69 Tg C. In the topsoil (0–10 cm), the PRCD was 152.31 g C m⁻²

and the PRCS was 13.58 Tg C, comprising 60% of the total PRCS. In the 10–20 cm and 20–30 cm soil layers, the PRCS capacities were 4.95 and 4.15 Tg C, comprising 22% and 18% of the total PRCS, respectively. The PRCD and PRCS in the different grassland types was analyzed (Figure 3c,d). In the 0–30 cm soil layer, mountain meadow ($453.31 \text{ g C m}^{-2}$) and temperate steppe ($419.95 \text{ g C m}^{-2}$) had distinctly higher PRCDs than the other grassland types. Mountain meadow and temperate steppe contributed approximately 30% of the total PRCS with capacities of 2.77 and 3.81 Tg C, respectively. Controlled by the area, temperate desert showed the largest capacity for PRCS at 12.72 Tg C (56% of the total).

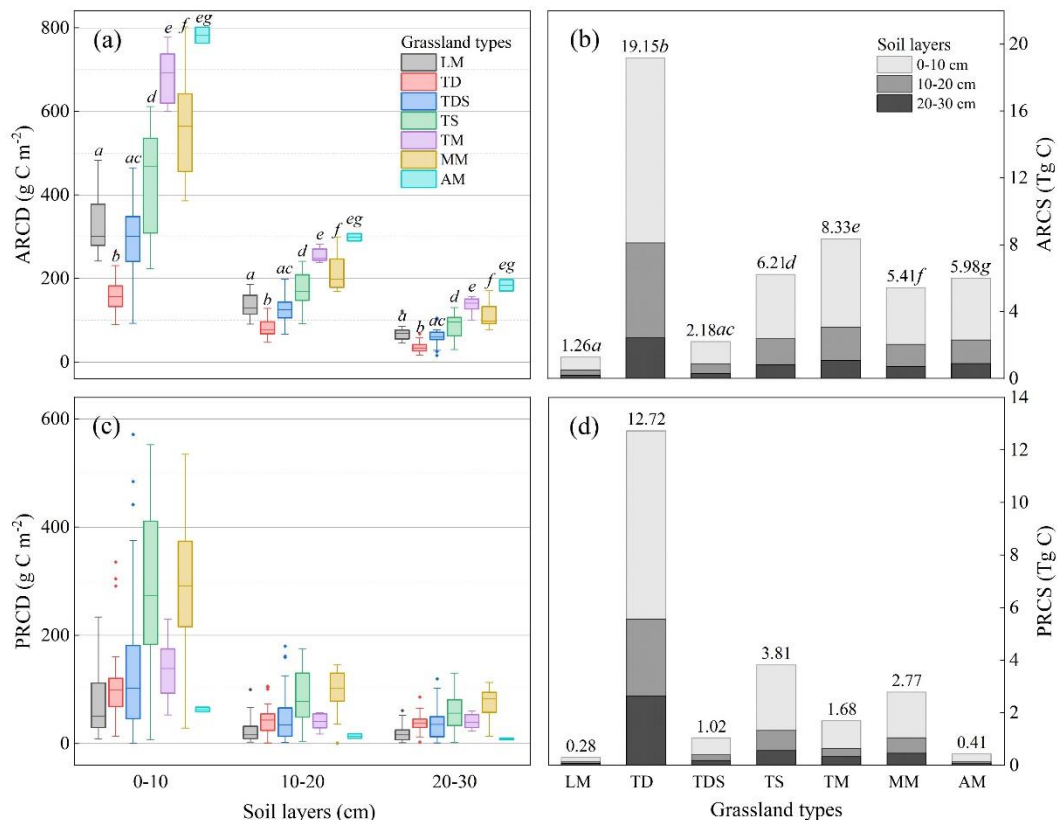


Figure 3. Statistical characteristics of root carbon in different grassland types in Altay Prefecture. (a,b) Actual root carbon density (ARCD) and actual root carbon storage (ARCS) of each grassland type; (c,d) potential root carbon density (PRCD) and potential root carbon storage (PRCS) of each grassland type. Different letters means statistically significant difference in the same same gene region. LM, lowland meadow; TD, temperate desert; TDS, temperate desert steppe; TS, temperate steppe; TM, temperate meadow; MM, mountain meadow; AM, alpine meadow.

The vertical changes in PRCS in the different grassland types was investigated (Figure 3c,d). The highest PRCS capacity was in the topsoil (0–10 cm) of different grassland types and ranged from 56–74%. Specifically, alpine meadow PRCS in the topsoil had the largest capacity and proportion of 0.30 Tg C and 74%, whereas temperate desert PRCS in the topsoil had the smallest capacity and proportion of 7.16 Tg C and of 56%. However, the opposite pattern was observed in the deeper soil layers. These results indicated that cold-season grasslands contained a higher proportion of PRCS in the topsoil than that of warm-season grasslands. Objectively, this phenomenon was affected by the formation mechanism and the vertical distribution of root biomass.

3.4. Spatial Drivers of Grassland ARCD and PRCD

Temperature and precipitation were the two dominant interaction factors for the spatial pattern of ARCD ($q = 0.77$; Figure 4a). The ARCD was significantly correlated with

shown remarkable performance in research fields such as the Internet, finance, agriculture [34], and medicine. In the present study, with consideration of multiple ecological factors, the grassland root biomass in complex terrain was successfully estimated using the SVM machine-learning model.

Subsequently, a high-performance spatial interpolation method was used for digital mapping in this research. Spatial interpolation is an effective approach for digital mapping [50]. However, it is often accompanied by a decrease in spatial accuracy [51]. Thus, it is necessary to compare the performance of the spatial interpolation methods used. Typically, some traditional interpolation methods identify targets based on the spatial distance or spatial autocorrelation (e.g., inverse-distance weighting and kriging) [52–54]. Other methods rely on continuous functions for interpolation of spatial points (e.g., trend surface method, RBF, and SPL). In the current study, the HASM spatial interpolation method was employed. This method optimizes the given interpolation outputs and their residuals using Lagrangian functions to improve the interpolation performance. Compared with RBF and SPL, HASM in practice shows superior performance with higher accuracy and lower error. In this study, a feasible combination of estimation model and spatial interpolation method was developed, namely ‘SVM + HASM’. This approach was applied for large-scale spatial study of grassland root biomass.

4.2. Spatial Pattern and Formation Mechanism of Grassland ARCD and ARCS

The grassland ARCD and ARCS in each soil layer in Altay Prefecture showed an analogous spatial pattern. Both indicators were high in mountains and low on plains, which is induced by rainfall in the Altai Mountains from precipitable water vapor originating from the Atlantic and Arctic Oceans. This phenomenon is widespread in the spatial pattern of plant carbon storage driven by topographic rainfall and temperature in the arid and semi-arid regions of the world [55,56]. Owing to strong topographic uplift, the hydrothermal environment and grassland types of mountains and plains show obvious heterogeneity with elevation. In addition, the ARCD showed vertical zonation. Therefore, temperate desert and temperate desert steppe, with low ARCD, were observed on plains limited by water availability and elevated temperature. The steppes and meadows with high ARCD were situated in mountains. Sufficient precipitation and cool temperatures extend the growth cycle of roots and delay carbon turnover [50,57]. An acceptable result is still obtained, although the stratified root carbon content rate is applied instead of the international one. The greatest capacity for root carbon storage is concentrated in the topsoil. This reflects the greater accumulation of organic matter in the surface soil [58]. Plant litter, animal carcasses, and animal excreta are decomposed by microorganisms, which increases the content of organic matter in the surface soil [59]. As a result, roots are attracted to access nutrients for plant growth and metabolism. The ARCD in the topsoil (0–10 cm) of different grassland types comprised 58–63% of the total capacity in the 0–30 cm soil layer, which was similar to previous results reported in other research fields [60–62].

4.3. Spatial Pattern and Dominated Drivers of Grassland PRCD and PRCS

We observed that in the 0–10 cm, 10–20 cm, and 20–30 cm soil layers, areas of high PRCD were located on the middle of southern slopes of the Altai Mountains. In addition, the PRCD declined with increase or decrease in elevation. Previous research has shown that water is the decisive driver of grassland PRCD [63,64]. The PRCD increases with enhanced precipitation and alpine meadow retains the highest PRCD. However, different results were obtained in the present study. Temperature was a controlling factor of the spatial pattern of PRCD in Altay Prefecture. Temperature is harmful to root growth when it exceeds the normal physiological tolerance [65]. The highest PRCD was located in mountain meadows rather than in alpine meadows. Generally, a mountain mid-slope with a suitable temperature is the optimal location for growth when the precipitation is sufficient to support prolonged growth in PRCD. This finding indicates that the interaction of hydrothermal factors is the most obvious exogenic force in the theory of their spatial pattern. Surprisingly,

the dominant interaction factors for this spatial pattern were temperature and slope, rather than temperature and precipitation, in the present study. Thus, slope contributes more to the spatial pattern of PRCD than does precipitation at a regional scale. Generally, compared with the plain pastures, mountain pastures showed a more obvious dependence on slope. In the present research, we presumed that grazing played an important role, although no empirical data are currently available to support this assumption. In Altay Prefecture, 1 million ha of summer pastures are dominated by mountain meadows [66]. These meadows are located at high elevations and on gentle slopes and are grazed by approximately 1.6 million livestock per year. We presumed that more carbonaceous organic material is transported to the aboveground organs in mountain meadows from belowground organs, which increases carbon investment in leaves, in response to grazing pressure [67–70]. This adaptive growth accordingly reduced the ARCD and considerably enhanced the PRCD capacity. In contrast, alpine meadow maintained a high ARCD as a result of the lower external disturbance and the PRCD remained limited.

5. Conclusions

In this study, a reliable approach for estimation of grassland root biomass in complex terrain was developed by combining the SVM model and HASM interpolation. The approach was applied to estimate the ARCS and PRCS of grassland in Altay Prefecture. Under the limitation of the hydrothermal environment, ARCD increased with elevation, and high ARCD was distributed mainly in the mountains and in the topsoil layer (0–10 cm). Simultaneously, high PRCD was distributed mainly on the middle of the southern slopes of the Altai Mountains. The dominant interaction factors were temperature and slope. The ARCS of the grassland comprised approximately 68% of the total root carbon storage, whereas PRCS comprised approximately 32% in the study area, suggesting that grassland in Altay Prefecture shows considerable capacity for increase in ARCS.

Author Contributions: Conceptualization, F.L.; methodology, F.L., Y.L. and X.Z.; software, F.L.; validation, F.L. and K.O.; formal analysis, F.L. and Y.L.; investigation, F.L. and H.Z.; resources, F.L. and H.Z.; data curation, F.L.; writing—original draft preparation, F.L.; writing—review and editing, H.Z., Y.L. and F.L.; visualization, F.L. and X.Z.; supervision, F.L. and K.O.; project administration, X.Z. and Y.L.; funding acquisition, X.Z. and Y.L. All authors have read and agreed to the published version of the manuscript.

Funding: The work was supported by the National Key R&D Program of China (2020YFD1100603-02), the National Science and Technology Foundation Work of China (2013FY110900, 2011FY110400), the National Natural Science Foundation of China (41971276), and the Graduate Innovation Foundation of Jiangxi Province (YC2020-B089), China.

Institutional Review Board Statement: Not applicable.

Informed Consent Statement: Not applicable.

Data Availability Statement: Not applicable.

Acknowledgments: This work was generated using data from the Geographic Sciences and Natural Resources Research, Chinese Academy of Sciences, funded at the site scale by professional researchers. We thank the experts of Jiangxi Agricultural University for their beneficial discussions.

Conflicts of Interest: The authors declare no conflict of interest.

References

1. Tang, X.; Zhao, X.; Bai, Y.; Tang, Z.; Wang, W.; Zhao, Y.; Wan, H.; Xie, Z.; Shi, X.; Wu, B.; et al. Carbon pools in China's terrestrial ecosystems: New estimates based on an intensive field survey. *Proc. Natl. Acad. Sci. USA* **2018**, *115*, 4021–4026. [[CrossRef](#)]
2. Hu, Z.; Song, X.; Wang, M.; Ma, J.; Zhang, Y.; Xu, H.; Hu, Z.; Zhu, X.; Liu, H.; Ma, J.; et al. Aridity influences root versus shoot contributions to steppe grassland soil carbon stock and its stability. *Geoderma* **2022**, *413*, 115744. [[CrossRef](#)]
3. Tessema, B.; Sommer, R.; Piikki, K.; Söderström, M.; Namirembe, S.; Notenbaert, A.; Tamene, L.; Nyawira, S.; Paul, B. Potential for soil organic carbon sequestration in grasslands in East African countries: A review. *Grassl. Sci.* **2022**, *66*, 135–144. [[CrossRef](#)]
4. Scurlock, J.M.O.; Hall, D.O. The global carbon sink: A grassland perspective. *Glob. Chang. Biol.* **1998**, *4*, 229–233. [[CrossRef](#)]

5. Yang, Y.; Tilman, D. Soil and root carbon storage is key to climate benefits of bioenergy crops. *Biofuel Res. J.* **2020**, *7*, 1143–1148. [[CrossRef](#)]
6. Yang, T.; Wu, X.; Wang, J.; Li, P.; Shi, H. Estimation of carbon storage in grassland ecosystem in China. *J. Arid Land Resour. Environ.* **2012**, *26*, 127–130. [[CrossRef](#)]
7. Mazzilli, S.R.; Kemanian, A.R.; Ernst, O.R.; Jackson, R.B.; Piñeiro, G. Greater humification of belowground than aboveground biomass carbon into particulate soil organic matter in no-till corn and soybean crops. *Soil Biol. Biochem.* **2015**, *85*, 22–30. [[CrossRef](#)]
8. Poeplau, C.; Germer, K.; Schwarz, K. Seasonal dynamics and depth distribution of belowground biomass carbon and nitrogen of extensive grassland and a *Miscanthus* plantation. *Plant Soil* **2019**, *440*, 119–133. [[CrossRef](#)]
9. Lorenz, K.; Lal, R. Carbon Sequestration in Grassland Soils. In *Carbon Sequestration in Agricultural Ecosystems*; Springer: Cham, Switzerland, 2018; pp. 175–209. [[CrossRef](#)]
10. Xia, J.; Liu, S.; Liang, S.; Chen, Y.; Xu, W.; Yuan, W. Spatio-temporal patterns and climate variables controlling of biomass carbon stock of global grassland ecosystems from 1982 to 2006. *Remote Sens.* **2014**, *6*, 1783–1802. [[CrossRef](#)]
11. Schimel, D.; Pavlick, R.; Fisher, J.B.; Asner, G.P.; Saatchi, S.; Townsend, P.; Miller, C.; Frankenberg, C.; Hibbard, K.; Cox, P. Observing terrestrial ecosystems and the carbon cycle from space. *Glob. Chang. Biol.* **2015**, *21*, 1762–1776. [[CrossRef](#)]
12. Sinha, S.; Jeganathan, C.; Sharma, L.K.; Nathawat, M.S. A review of radar remote sensing for biomass estimation. *Int. J. Environ. Sci. Technol.* **2015**, *12*, 1779–1792. [[CrossRef](#)]
13. Bartholomé, O.; Grigulis, K.; Colace, M.; Arnoldi, C.; Lavorel, S. Methodological uncertainties in estimating carbon storage in temperate forests and grasslands. *Ecol. Indic.* **2018**, *95*, 331–342. [[CrossRef](#)]
14. Zhao, Z.; Liu, G.; Mou, N.; Xie, Y.; Xu, Z.; Li, Y. Assessment of carbon storage and its influencing factors in Qinghai-Tibet Plateau. *Sustainability* **2018**, *10*, 1864. [[CrossRef](#)]
15. Viglizzo, E.F.; Ricard, M.F.; Taboada, M.A.; Vázquez-Amábile, G. Reassessing the role of grazing lands in carbon-balance estimations: Meta-analysis and review. *Sci. Total Environ.* **2019**, *661*, 531–542. [[CrossRef](#)] [[PubMed](#)]
16. Zhang, C. Study on Carbon Budget of Grassland Ecosystem by DNDC Model. Ph.D. Thesis, Inner Mongolia Normal University, Hohhot, China, 2020.
17. Husáková, I.; Weiner, J.; Münzbergová, Z. Species traits and shoot-root biomass allocation in 20 dry-grassland species. *J. Plant Ecol.* **2016**, *11*, 273–285. [[CrossRef](#)]
18. Milchunas, D.G. Estimating Root Production: Comparison of 11 methods in shortgrass steppe and review of biases. *Ecosystems* **2009**, *12*, 1381–1402. [[CrossRef](#)]
19. Ferraz, A.; Saatchi, S.; Xu, L.; Hagen, S.; Chave, J.; Yu, Y.; Meyer, V.; Garcia, M.; Silva, C.; Roswintart, O.; et al. Carbon storage potential in degraded forests of Kalimantan, Indonesia. *Environ. Res. Lett.* **2018**, *13*, 95001. [[CrossRef](#)]
20. Hariyadi; Mahulette, A.S.; Yahya, S.; Wachjar, A. Measuring the potential of biomass, carbon storage, and carbon sink of forest cloves. *IOP Conf. Ser. Earth Environ. Sci.* **2019**, *399*, 12063. [[CrossRef](#)]
21. Song, Z.; Wu, Y.; Yang, Y.; Zhang, X.; van Zwieten, L.; Bolan, N.; Li, Z.; Liu, H.; Hao, Q.; Yu, C.; et al. High potential of stable carbon sequestration in phytoliths of China's grasslands. *Glob. Chang. Biol.* **2022**, *28*, 2736–2750. [[CrossRef](#)]
22. Li, Y.; Chen, K.; Zheng, N.; Cai, Q.; Li, Y.; Lin, C. Strategy research on accelerating green and low-carbon development under the guidance of carbon peak and carbon neutral targets. *IOP Conf. Ser. Earth Environ. Sci.* **2021**, *793*, 12009. [[CrossRef](#)]
23. Wang, Y.; Guo, C.; Du, C.; Chen, X.; Jia, L.; Guo, X.; Chen, R.; Zhang, M.; Chen, Z.; Wang, H. Carbon peak and carbon neutrality in China: Goals, implementation path, and prospects. *China Geol.* **2021**, *4*, 720–746. [[CrossRef](#)]
24. Li, Z.; Huffman, T.; McConkey, B.; Town-Smith, L. Monitoring and modeling spatial and temporal patterns of grassland dynamics using time-series MODIS NDVI with climate and stocking data. *Remote Sens. Environ.* **2013**, *138*, 232–244. [[CrossRef](#)]
25. Li, M. *Carbon Storages and Carbon Sequestration Potentials of the Terrestrial Ecosystems on the Loess Plateau*; Chinese Academy of Sciences and Ministry of Education (Research Center of Research Center Soil and Water Conservation and Ecological Environment): Beijing, China, 2021.
26. Du, Y.; Zhou, G.; Guo, X.; Cao, G. Spatial distribution of grassland soil organic carbon and potential carbon storage on the Qinghai Plateau. *Grassl. Sci.* **2019**, *65*, 141–146. [[CrossRef](#)]
27. Poeplau, C. Estimating root: Shoot ratio and soil carbon inputs in temperate grasslands with the RothC model. *Plant Soil* **2016**, *407*, 293–305. [[CrossRef](#)]
28. Yu, X.; Li, C.; Chen, H.; Yu, X. Evaluate the effectiveness of multi objective evolutionary algorithms by box plots and fuzzy TOPSIS. *Int. J. Comput. Intell. Syst.* **2019**, *12*, 733. [[CrossRef](#)]
29. Navarro, J. Bivariate box plots based on quantile regression curves. *Depend. Model.* **2020**, *8*, 132–156. [[CrossRef](#)]
30. Hoese, T.; Kuenzer, C. Object detection and image segmentation with deep learning on earth observation data: A review-part I: Evolution and recent trends. *Remote Sens.* **2020**, *12*, 1667. [[CrossRef](#)]
31. Chen, X.; Li, S.; Mersch, B.; Wiesmann, L.; Gall, J.; Behley, J.; Stachniss, C. Moving Object Segmentation in 3D LiDAR Data: A Learning-based approach exploiting sequential data. *IEEE Robot. Autom. Lett.* **2021**, *6*, 6529–6536. [[CrossRef](#)]
32. Ray, S. A quick review of machine learning algorithms. In Proceedings of the 2019 International Conference on Machine Learning, Big Data, Cloud and Parallel Computing (Com-IT-Con), Faridabad, India, 14–16 February 2019.
33. Jafar Alzubi, A.N.A.K. Machine learning from theory to algorithms: An overview. *J. Phys. Conf. Ser.* **2018**, *1142*, 12012. [[CrossRef](#)]
34. Liakos, K.; Busato, P.; Moshou, D.; Pearson, S.; Bochtis, D. Machine learning in agriculture: A review. *Sensors* **2018**, *18*, 2674. [[CrossRef](#)] [[PubMed](#)]

35. Carleo, G.; Cirac, I.; Cranmer, K.; Daudet, L.; Schuld, M.; Tishby, N.; Vogt-Maranto, L.; Zdeborová, L. Machine learning and the physical sciences. *Rev. Mod. Phys.* **2019**, *91*, 1. [[CrossRef](#)]
36. Sarker, I.H. Machine learning: Algorithms, real-world applications and research directions. *SN Comput. Sci.* **2021**, *2*, 160. [[CrossRef](#)]
37. Chauhan, V.K.; Dahiya, K.; Sharma, A. Problem formulations and solvers in linear SVM: A review. *Artif. Intell. Rev.* **2019**, *52*, 803–855. [[CrossRef](#)]
38. Zou, H.; Xue, L. A selective overview of sparse principal component analysis. *Proc. IEEE* **2018**, *106*, 1311–1320. [[CrossRef](#)]
39. Wu, S.; Hannig, J.; Lee, T.C.M. Uncertainty quantification for principal component regression. *Electron. J. Stat.* **2021**, *15*, 2157–2178. [[CrossRef](#)]
40. Borup, D.; Christensen, B.J.; Mühlbach, N.N.; Nielsen, M.S. Targeting predictors in random forest regression. *Int. J. Forecast.* **2019**. [[CrossRef](#)]
41. Tian, Z.; Liu, F.; Liang, Y.; Zhu, X. Mapping soil erodibility in southeast China at 250 m resolution: Using environmental variables and random forest regression with limited samples. *Int. Soil Water Conserv. Res.* **2022**, *10*, 62–74. [[CrossRef](#)]
42. Amini, M.A.; Torkan, G.; Eslamian, S.; Zareian, M.J.; Adamowski, J.F. Correction to: Analysis of deterministic and geostatistical interpolation techniques for mapping meteorological variables at large watershed scales. *Acta Geophys.* **2019**, *67*, 275. [[CrossRef](#)]
43. Wang, S.; Fan, J.; Zhong, H.; Li, Y.; Zhu, H.; Qiao, Y.; Zhang, H. A multi-factor weighted regression approach for estimating the spatial distribution of soil organic carbon in grasslands. *CATENA* **2019**, *174*, 248–258. [[CrossRef](#)]
44. Yue, T.; Du, Z.; Song, D.; Gong, Y. A new method of surface modeling and its application to DEM construction. *Geomorphology* **2007**, *91*, 161–172. [[CrossRef](#)]
45. Wang, G.; Chen, X.; Liu, Z. Mesh deformation on 3D complex configurations using multistep radial basis functions interpolation. *Chin. J. Aeronaut.* **2018**, *31*, 660–671. [[CrossRef](#)]
46. Kätterer, T.; Bolinder, M.A.; Andrén, O.; Kirchmann, L.; Menichetti, L. Roots contribute more to refractory soil organic matter than above-ground crop residues, as revealed by a long-term field experiment. *Agric. Ecosyst. Environ.* **2011**, *141*, 184–192. [[CrossRef](#)]
47. Ji, O.; He, J.; Jiang, Q. Characteristics and composition of vegetation carbon storage in natural grassland in Ning-Xia, China. *Chin. J. Appl. Ecol.* **2021**, *32*, 1259–1268. [[CrossRef](#)]
48. Zhao, Y.; Liu, L.; Kang, S.; Ao, Y.; Han, L.; Ma, C. Quantitative analysis of factors influencing spatial distribution of soil erosion based on Geo-detector model under diverse geomorphological types. *Land* **2021**, *10*, 604. [[CrossRef](#)]
49. Tang, Z.; Deng, L.; An, H.; Shangguan, Z. Bayesian method predicts belowground biomass of natural grasslands. *Écoscience* **2017**, *24*, 127–136. [[CrossRef](#)]
50. Wang, N.; Quesada, B.; Xia, L.; Butterbach Bahl, K.; Goodale, C.L.; Kiese, R. Effects of climate warming on carbon fluxes in grasslands—A global meta-analysis. *Glob. Chang. Biol.* **2019**, *25*, 1839–1851. [[CrossRef](#)]
51. Li, H.; Shao, Z. Review of spatial interpolation analysis algorithm. *Comput. Syst. Appl.* **2019**, *28*, 1–8. [[CrossRef](#)]
52. Blanco, I.; Diego, I.; Bueno, P.; Fernandez, E.; Casas-Maldonado, F.; Esquinas, C.; Soriano, J.B.; Miravittles, M. Geographical distribution of COPD prevalence in Europe, estimated by an inverse distance weighting interpolation technique. *Int. J. COPD* **2018**, *13*, 57–67. [[CrossRef](#)] [[PubMed](#)]
53. Wu, W.; Gan, R.; Li, J.; Cao, X.; Ye, X.; Zhang, J.; Qu, H. A spatial interpolation of meteorological parameters considering geographic semantics. *Adv. Meteorol.* **2020**, *2020*, 9185283. [[CrossRef](#)]
54. Munyati, C.; Sinthumule, N.I. Comparative suitability of ordinary kriging and inverse distance weighted interpolation for indicating intactness gradients on threatened savannah woodland and forest stands. *Environ. Sustain. Indic.* **2021**, *12*, 100151. [[CrossRef](#)]
55. Leng, R.; Yuan, Q.; Wang, Y.; Kuang, Q.; Ren, P. Carbon balance of grasslands on the Qinghai-Tibet Plateau under future climate change: A review. *Sustainability* **2020**, *12*, 533. [[CrossRef](#)]
56. Jaman, M.S.; Wu, H.; Yu, Q.; Tan, Q.; Zhang, Y.; Dam, Q.K.; Muraina, T.O.; Xu, C.; Jing, M.; Jia, X.; et al. Contrasting responses of plant above and belowground biomass carbon pools to extreme drought in six grasslands spanning an aridity gradient. *Plant Soil* **2022**, *473*, 167–180. [[CrossRef](#)]
57. Xia, J.; Ma, M.; Liang, T.; Wu, C.; Yang, Y.; Zhang, L.; Zhang, Y.; Yuan, W. Estimates of grassland biomass and turnover time on the Tibetan Plateau. *Environ. Res. Lett.* **2017**, *13*, 14020. [[CrossRef](#)]
58. Jobbágy, E.G.; Jackson, R.B. The vertical distribution of soil organic carbon and its relation to climate and vegetation. *Ecol. Appl.* **2000**, *10*, 423–436. [[CrossRef](#)]
59. Six, J.; Elliott, E.T.; Paustian, K.; Doran, J.W. Aggregation and soil organic matter accumulation in cultivated and native grassland soils. *Soil Sci. Soc. Am. J.* **1998**, *62*, 1367–1377. [[CrossRef](#)]
60. Gu, Q.; Wei, J.; Luo, S.; Ma, M.; Tang, X. Potential and environmental control of carbon sequestration in major ecosystems across arid and semi-arid regions in China. *Sci. Total Environ.* **2018**, *645*, 796–805. [[CrossRef](#)]
61. Niu, B.; Zeng, C.; Zhang, X.; He, Y.; Shi, P.; Tian, Y.; Feng, Y.; Li, M.; Wang, Z.; Wang, X.; et al. High below-ground productivity allocation of alpine grasslands on the northern Tibet. *Plants* **2019**, *8*, 535. [[CrossRef](#)]
62. Garcia-Pausas, J.; Casals, P.; Romanyà, J.; Vallecillo, S.; Sebastià, M. Seasonal patterns of belowground biomass and productivity in mountain grasslands in the Pyrenees. *Plant Soil* **2011**, *340*, 315–326. [[CrossRef](#)]
63. Ma, W.H.; Yang, Y.H.; He, J.S.; Zeng, H.; Fang, J.Y. Above-and belowground biomass in relation to environmental factors in temperate grasslands, Inner Mongolia. *Sci. China Ser. C Life Sci.* **2008**, *51*, 263–270. [[CrossRef](#)]

64. Kang, M.; Dai, C.; Ji, W.; Jiang, Y.; Yuan, Z.; Chen, H.Y.H. Biomass and its allocation in relation to temperature, precipitation, and soil nutrients in Inner Mongolia grasslands, China. *PLoS ONE* **2013**, *8*, e69561. [[CrossRef](#)]
65. Kaspar, T.C.; Bland, W.L. Soil temperature and root growth. *Soil Sci.* **1992**, *154*, 290–299. [[CrossRef](#)]
66. Li, F. Study on Grassland Biomass by Gridding Approach: A Case Study of Altay Region, Xinjiang. Master's Thesis, Jiangxi Agricultural University, Nanchang, China, 2019.
67. Van der Maarel, E.; Titlyanova, A. Above-ground and below-ground biomass relations in Steppes under different grazing conditions. *Oikos* **1989**, *56*, 364. [[CrossRef](#)]
68. Chang, Q.; Wang, L.; Ding, S.; Xu, T.; Li, Z.; Song, X.; Zhao, X.; Wang, D.; Pan, D. Grazer effects on soil carbon storage vary by herbivore assemblage in a semi-arid grassland. *J. Appl. Ecol.* **2018**, *55*, 2517–2526. [[CrossRef](#)]
69. Sarquis, A.; Pestoni, S.; Cingolani, A.M.; Pérez Harguindeguy, N. Physiognomic changes in response to herbivory increase carbon allocation to roots in a temperate grassland of central Argentina. *Plant Ecol.* **2019**, *220*, 699–709. [[CrossRef](#)]
70. Zhou, G.; Luo, Q.; Chen, Y.; He, M.; Zhou, L.; Frank, D.; He, Y.; Fu, Y.; Zhang, B.; Zhou, X. Effects of livestock grazing on grassland carbon storage and release override impacts associated with global climate change. *Glob. Chang. Biol.* **2019**, *25*, 1119–1132. [[CrossRef](#)]